Dynamics of viscous-fingering fractals in porous media

Knut Jørgen Måløy, Finn Boger, Jens Feder, and Torstein Jøssang
Institute of Physics, University of Oslo, P.O. Box 1048, Blindern, N-0316 Oslo 3, Norway

Paul Meakin
Central Research and Development Department, E. I. du Pont de Nemours and Company, Inc., Experimental Station, Wilmington, Delaware 19898

(Received 1 December 1986)

A gas displacing a high-viscosity liquid in a porous medium generates a fractal finger structure similar to that obtained in diffusion-limited aggregation (DLA). This structure is controlled by the surface dynamics of the growing active zone. The dynamics of viscous fingering in a two-dimensional porous model has been investigated. We have studied the radius of the active zone and the screening length of the active zone as a function of time in the DLA regime. In this regime the fingering structure grows mainly at the tips, and the inner region is screened by the outer fingers. The length of the longest finger as a function of time is accurately described by the results of a *new* form of DLA simulation which in addition to DLA structures gives the time dependence in a form suitable for comparison with experiments.

I. INTRODUCTION

The displacement of a high-viscosity fluid by a low-viscosity fluid in a porous medium in a process of both scientific and practical importance. It has recently been shown by Chen and Wilkinson[1] and by Måløy, Feder, and Jøssang[2] that viscous fingering in a random porous medium at high capillary numbers $\mathcal{C} \gg 10^{-4}$ generates structures with a fractal[3] geometry. This fractal structure closely resembles that obtained from the diffusion-limited-aggregation (DLA) model of Witten and Sander.[4] Similar structures have also been obtained by fluid-fluid displacement in radial Hele-Shaw cells using non-Newtonian viscous fluids.[5] The relationship between fluid-fluid displacement in porous media and DLA was first discussed by Paterson[6] and a more detailed analysis has been presented by Kadanoff.[7]

A wide variety of non-equilibrium processes, such as dielectric breakdown,[8] electrodeposition,[9,10] random dendritic growth,[11,12] and the dissolution of porous materials[13] has also been shown to lead the formation of structures similar to those associated with the DLA model. Here we describe a study of viscous fingering of Newtonian fluids in a porous medium at high capillary numbers ($\mathcal{C} = u\mu/\sigma \simeq 0.15$). Here u is the mean velocity of the longest finger, μ is the viscosity of the viscous liquid, and σ is the surface tension. Under these conditions growth occurs mainly at the relatively unscreened (most exposed) tips of the fingers and can be described in terms of an active zone[14] which leaves behind a "frozen" structure that does not evolve further with increasing time. Since the frozen interior, which forms the majority of the cluster, is formed by the advance of the active zone, it is reasonable to expect that a more complete description of the dynamics of the active zone might lead to a better understanding of the viscous finger structure.

The original DLA model of Witten and Sander specifies a time-ordered sequence of events but is not explicitly time dependent. While the time-dependent aspects of DLA and closely related processes have been explored theoretically[15,16] and by means of computer simulations,[17,18] this aspect of DLA has only recently been explored experimentally.[2]

Here we describe the results of experiments carried out to explore the dynamics of fluid-fluid displacement in a two-dimensional (2D) porous medium. The results of these experiments are compared with simulations carried out using a modified DLA model which allows the time dependence of the growth process to be investigated in the zero concentration limit.

II. EXPERIMENTAL METHODS

The experimental setup is shown in Fig. 1. The porous model consists of 1-mm glass spheres sandwiched between a stiff plexiglass disk and a thin plastic sheet held in con-

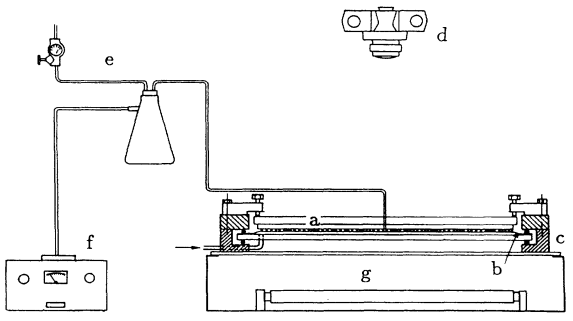

FIG. 1. Experimental setup. *a*, porous model with glass spheres; *b*, plastic film; *c*, external aluminum ring; *d*, camera; *f*, pressure gauge; *e*, pressure reduction system; *g*, light board.

tact with the spheres by compressed air. The model was made by coating a Plexiglass disc (6 mm thick and 40 cm in diameter) with a 0.1-mm layer of transparent epoxy, and spreading a layer of 1-mm glass spheres onto the disk. The epoxy was allowed to partially harden before spreading the glass spheres so that the spheres would stick on contact and not move later. After the epoxy layer hardened, the excess of glass spheres was removed, leaving a monolayer. The disc with the monolayer of spheres is placed, face down, onto a plastic film. This assembly is supported from above and below by 10-mm-thick glass discs and clamped in an aluminum ring, as illustrated in Fig. 1. We connected the space between the plastic film and the lower glass plate to a compressed air supply in order to force the film into contact with all of the glass spheres. This air pressure was higher than the pressure of the air injected into the porous model, and was held constant during the experiment. Filling the model before increasing the pressure on the plastic film, makes it easier to fill pores with high-viscosity fluids without trapping air bubbles.

In a typical experiment, air injected at the center displaces glycerol, filling the pore space of the model. Air at a constant pressure is introduced into the porous layer through a 1-mm hole at the center of the Plexiglass disc. A stable pressure of the air displacing the glycerol was obtained using a Mortanair B11-M3 pressure regulator and a Norgren low-pressure regulator connected with an external reservoir of about 5 l. The pressure of the air during the injection process was measured with a Texas Instrument fused quartz pressure gauge, and the pressure fluctuations at the center were typically less than 0.5%.

The resulting finger structure was photographed with a Nikon F3 camera controlled from an IBM PC XT (personal computer). Uniform lighting on the transparent model was provided from below. A typical time between each picture was 0.6 s. The pictures were enlarged using an Agfa Gevaert Reprodoline 716 transparent film. Figure 2 shows a typical viscous finger pattern obtained in this way. Note that the picture in Fig. 2 is obtained by superimposing a negative picture of the filled model with a positive picture of the finger structure. We thus subtract out all the features that remain constant such as the fixed spheres and any uneveness in the illumination. In effect we obtain the difference between the two pictures.

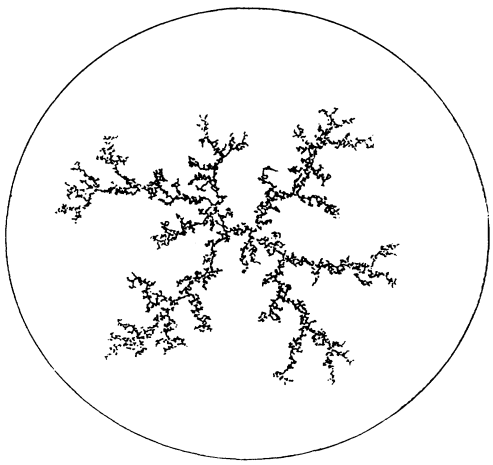

FIG. 2. Fractal viscous fingering with a fractal dimension $D=1.64\pm0.04$ in a two-dimensional porous medium. Air was injected in glycerol with a pressure (p_s-p_0) of 20.2 mm Hg and a capillary number $\mathcal{C}$ of 0.15.

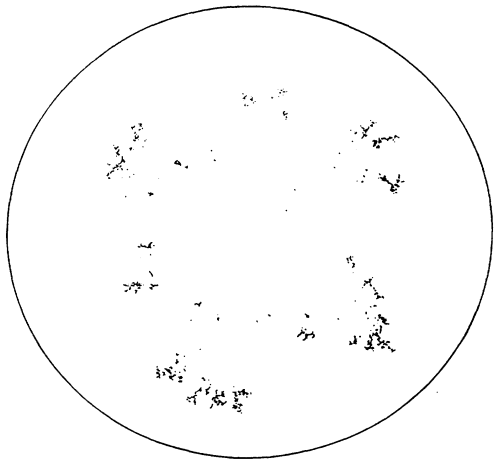

FIG. 3. Active zone of a viscous fingering structure in a two-dimensional porous model. The time between each picture used to construct this picture of the growth zone is 2.6 s. Air was injected in glycerol with a pressure (p_s-p_0) of 20.2 mm Hg and capillary number $\mathcal{C}$ of 0.15.

In order to identify the active growth zone at a given time, and to filter out noise from the picture, we subtracted the picture taken at the previous time. The earlier picture was subtracted by superimposing the negative of the earlier picture below the positive of the last picture. In this way we obtained the growth zone shown in Fig. 3, for the finger structure shown in Fig. 2.

The viscous fingers were analyzed by digitizing the pictures using an RCA TC2055CX video camera and a Tecmar Video van Gogh interface in an IBM PC. The resolution of this equipment is 256×256 pixels.

III. COMPUTER SIMULATION

The original lattice model of Witten and Sander[4] for diffusion-limited aggregation was modified to represent the displacement of a viscous fluid by a nonviscous fluid in a two-dimensional porous medium of finite size. The modified model which was used for this purpose is illustrated in Fig. 4. Figure 4 represents an early stage in a small-scale simulation on a square lattice. The sites which are occupied by the zero-viscosity fluid are shaded and the growth sites (unoccupied sites with one or more occupied nearest neighbors) are represented by open squares. To simulate the viscous fingering process, one of the unoccupied surface sites is selected at random and the random walk is started from that site. After each random walker is launched from an unoccupied surface site, the simulation time is incremented by $1/N_s$ where N_s is the total number of surface sites. The random-walk trajectory is stopped and the site from which the random walk originated is filled if the random walker moves a distance

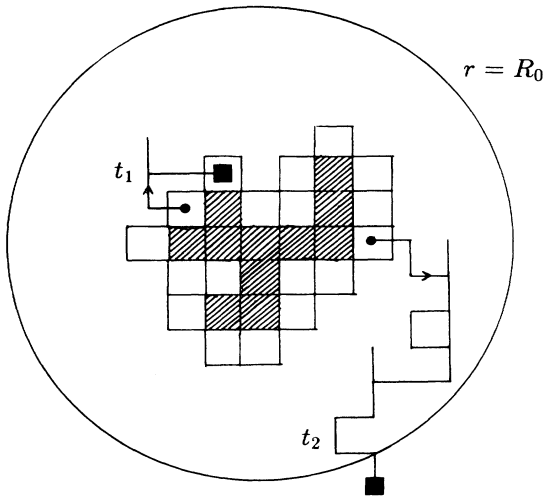

FIG. 4. Schematic representation of the model used to simulate fluid-fluid displacement in a two-dimensional porous medium. The shaded sites on the square lattice represent regions occupied by a nonviscous fluid. The unoccupied surface sites are represented by open squares and the rest of the regions occupied by the viscous Newtonian fluid is blank. Two typical random-walk trajectories (t_1 and t_2) are shown. The origin of each trajectory is indicated by a dot and the termination is indicated by a square. Trajectory t_1 reaches the edge of the "cell" at a radius of $r = R_0$ and the site at its origin is filled. Trajectory t_2 returns to the cluster and does not result in growth. The original "seed" or growth site which represents the point at which the nonviscous fluid is injected is darkly shaded.

greater than R_0 from the original seed or growth site. The circle of radius $r = R_0$ represents the edge of the cell. The random-walk trajectory t_1 in Fig. 4 shows a random walk which results in growth. If the random-walk trajectory reaches a second unoccupied surface site, the random walk is stopped but growth does not occur; this process is represented by trajectory t_2 in Fig. 4. After each random walk has terminated a new random walk is started at a randomly selected surface site and the time is incremented by $1/N_s$. The simulation is continued until the growth reaches the edge of the cell.

This model is based on the equivalence of a field obeying Laplace's equation [in this case the pressure field $p(\mathbf{r})$] and particles undergoing random walks subject to the same boundary conditions. The pressure field $p(\mathbf{r})$ at position $\mathbf{r}$ is proportional to the number of times the lattice site at position $\mathbf{r}$ is visited by the random walkers. By starting the random walkers with equal probability at each of the unoccupied surface sites and terminating them if they return to the surface, we satisfy the boundary conditions $p(\mathbf{r}_s) = p_s = \text{const}$ for all the surface sites. Termination of the random walkers at the outer boundary with a radius of R_0 corresponds to the boundary condition $p(\mathbf{r}_0) = p_0 = 0$ for all the positions at the edge of the cell.

In our simulation the random walkers are launched at a constant rate from all of the surface sites. Consequently, the simulations correspond to experiments in which a constant pressure difference is maintained across the viscous fluid. The total number of particles ΔN launched from the cluster surface within a time interval Δt is proportional to the pressure $p_s = \text{const}$ at the surface times the total number of surface particles N_s. We then get the time interval $\Delta t \sim \Delta N / N_s$ used in the simulations. In Fig. 4 the model is illustrated for the case of a square lattice. In practice, a hexagonal lattice was used to minimize the effects of lattice anisotropy.[19]

The simulations could equally well have been carried out by launching the random walkers from the outer boundary representing the edge of the cell. In this case the time would be incremented by a constant amount ($1/N_b$ where N_b is the number of sites at the outer boundary) after each walker had been launched. In the early stages of simulation most of the walkers would return to the outer boundary (and be removed) before contacting the growing cluster. Growth would occur each time a random walker reached the surface of the cluster. The equivalence of these two simulation methods is a result of microscopic reversibility under the quasistationary growth conditions which are assumed in these models. Growth occurs each time a path connecting the cluster to the outer boundary is found. Because of the time-reversal symmetry of random walks, each path has an equal probability of being found in both simulation methods.

At early stages in these simulations, random walkers launched from the outer boundary would have a low probability of reaching the cluster and there would be many time increments between each growth event. If the random walkers were launched from the cluster, there would be a higher probability of finding the outer boundary but the time increments would be large because there would be few surface sites at this stage. In the later stages of growth many of the random walkers launched from the cluster would originate from well-screened interior sites, but almost all of these would recontact the cluster before reaching the outer boundary. At this stage the time increments are small but a relatively large number of random walkers must be launched in order for one of them to reach the outer boundary.

In order to improve the efficiency of the simulation, the random walkers were allowed to make large off-lattice jumps when they were a long distance from both the cluster and the outer boundary.[20] If the random walker is at a distance s from the nearest occupied site on either the cluster or the outer boundary, a move by a distance which is a few lattice distances smaller than s was permitted in any direction. In the vicinity of either the cluster or the outer boundary the random walker was transferred to the nearest lattice site and moved via lattice steps until it either reached a boundary or moved a longer distance from both the cluster and the outer boundary. Despite the improvements resulting from this procedure, quite large amounts of computer time are required for these relatively small-scale simulations.

IV. GROWTH OF VISCOUS FINGERS

Saffman and Taylor[21] developed a theory of viscous fingering in a Newtonian liquid between two plates of gap

a with rectangular symmetry. They supposed that the fluid is described by Darcy's law

$$\mathbf{U}=\frac{k}{\mu}\nabla p \tag{1}$$

for each of the two fluids separately. $\mathbf{U}$ is the fluid flux and $k=a^2/12$ the permeability. Paterson[22] solved the same problem for a 2D circular Hele-Shaw cell and found that, when the circumference increases beyond a critical value $\lambda_c/a=\mathcal{C}^{-1/2}$, it becomes unstable and splits into fingers with a width of λ_c. However, the structure of viscous fingers in a porous medium is fractal, and is therefore qualitatively different from the structures in an ordinary Hele-Shaw cell which is not fractal at the same capillary numbers.

For an incompressible fluid and a porous medium with homogeneous porosity, Darcy's law equation (1) and $\nabla\cdot\mathbf{U}=0$ gives the Laplace equation

$$\nabla^2 p=0\ . \tag{2}$$

Here we are concerned with a gas injected with a constant pressure p_s and with constant pressure p_0 at the rim. The ordinary Hele-Shaw cell and a Hele-Shaw cell with a porous medium will satisfy the same differential equations [(1) and (2)]. However, the boundary conditions are clearly not the same. In the case of a porous medium a new length scale, the size of the pore b, must be taken into account. In a porous medium, the direction of the propagation and the width of the viscous fingers depend on the pore size and the geometry of the porous matrix. In an ordinary Hele-Shaw cell, the finger width is controlled by λ_c. Note that Darcy's equation (1) only applies in an averaged sense, and the permeability k is defined only when one considers the porous medium on length scales much larger than typical pore dimensions. The dynamics of displacement fronts which advance on the pore level is therefore not described by the Darcy equation alone, and the random pore geometry influences the displacement dynamics.

Nittmann, Daccord, and Stanley[5] have studied viscous fingering of water into a non-Newtonian liquid with zero interface tension. Using a radial Hele-Shaw cell they found a fractal dimension $D=1.7$ consistent with our result and the DLA result. On the other hand, there are differences between the structure they observed and the finger structure generated in a random porous medium. One difference is that their main branches tend to be much more straight and do not have the same treelike structure as seen in Fig. 2. Another important difference is that their side branches grow with an angle very near 40° out from the main branches. In the random model the viscous fingers grow in a direction determined by the porous matrix and the largest pressure gradients at the interface between the two fluids, and do not have a narrow angular distribution.

In a continuum description of fluid-fluid displacement the fingers will grow in the regions where the pressure gradient at the interface is largest. In the diffusion-limited-aggregation model an additional component is introduced by the stochastic nature of the random walk. In a random porous medium the pressure gradients across the pore necks will fluctuate along the interface because of the capillary pressure fluctuations and the viscous drag fluctuations at the pore level. This pressure fluctuation is important and should not be neglected, even at high capillary numbers. To understand the dynamics of viscous fingers at high capillary numbers, it is therefore important to consider both the global pressure given by Darcy's law and the pressure fluctuations at the pore level.

In Fig. 2 the result of an experiment at a capillary number $\mathcal{C}$ of 0.15 is shown. The fractal dimension of this cluster is $D=1.64\pm0.04$. The viscous fingering structure was analyzed by digitizing pictures such as that shown in Fig. 2. The number $N(r)$ of black pixels was calculated as a function of distance r, from a point near the injection center. We expect $N(r)$ to have the scaling form

$$N(r)=N_0(r/R_g)^D f(r/R_g)\ . \tag{3}$$

Here, R_g is the radius of gyration and N_0 is the total number of black pixels. The crossover function $f(x)$ is constant in the range $a/R_g<x<1$ and tends to x^{-D} for $x>1$, and we find $N(r)\to N_0$ for $r\gg R_g$. In Fig. 5 we plot $\log_{10}[N(r)/N_0]$ as a function of $\log_{10}(r/R_g)$ for the structure shown in Fig. 2. By fitting Eq. (3) in the range $2a<r<R_g$, we find a fractal dimension $D=1.64\pm0.04$. This value is the mean value of D obtained by choosing different centers (on the cluster) inside an area with a radius of a about 8 pixels from the center of injection. The uncertainty given expresses the range of D values obtained within this area. This value for the fractal dimension differs somewhat from that obtained from simulation results[23] ($D\simeq1.71$). However, the shape of the viscous fingers shown in Fig. 2 bears a striking resemblance to the shapes generated by two-dimensional DLA models and we believe that a DLA model describes the essential physics of our experiments.

One important feature of the pressure field given by Darcy's law is the screening of the inner region by the longest fingers. This is easily seen in Fig. 3 where almost all the growth is at the tips. In Fig. 6 the distance r_m

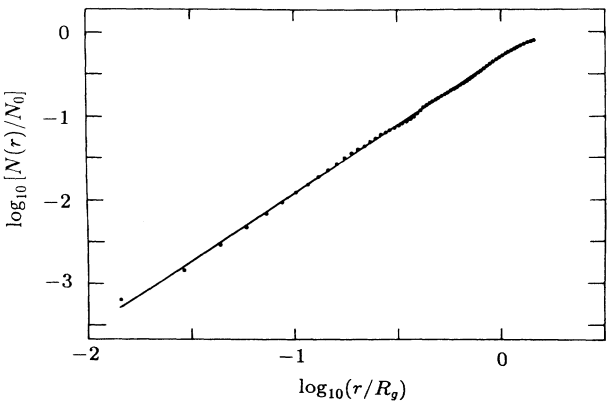

FIG. 5. Normalized finger structure area $N(r)/N_0$ as a function of the reduced radius r/R_g. Experiment on glycerol at $\mathcal{C}=0.15$. The solid line, obtained from a linear fit to the experimental data, has a slope of 1.64.

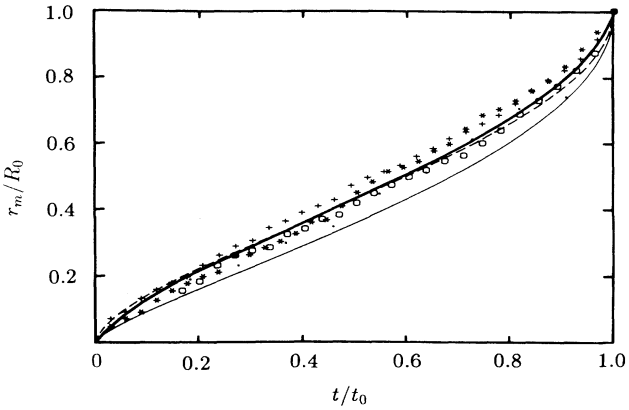

FIG. 6. Length r_m/R_0 of the longest finger as a function of time t/t_0. Four experiments on a two-dimensional system of 1-mm glass spheres. The dashed curve is Eq. (4), the thin solid curve represents the same equation but with exponent 1.64. The thick solid curve is the result of our simulations.

from the center of injection to the tip of the longest finger is plotted as a function of t/t_0, where t_0 is the breakthrough time when $r_m = R_0$ and t is the time when the picture was taken. Four different experiments with the same pressure p_s at the center of injection and the same size of glass spheres (1 mm in diameter) are shown. For a circular bubble of radius r at a fixed pressure p_s expanding into the viscous fluids, Eqs. (1) and (2) give the relation

$$t/t_0 = (r/R_0)^2[1 - \ln(r/R_0)^2] \ . \tag{4}$$

This gives the dashed curve in Fig. 6, and it describes the data well. This indicates that the longest fingers control the potential flow and generate a "Faraday cage" with a radius almost equal to r_m screening the internal structure of shorter fingers. Clearly, Eq. (4) should be modified for fractal growth. Matsushita *et al.*[9] studied the fractal structure of two-dimensional zinc-metal leaves grown by electrodeposition and obtained $D = 1.66 \pm 0.03$. They proposed that the "effective" radius of the structure should grow as $r \sim t^{1/D}$. This proposal suggests that the exponent 2 in Eq. (4) be replaced by D, in order to account for the fact that less of the fluid is displaced by fractals than by a bubble. This replacement gives the thin fully drawn curve in Fig. 6. We expect this replacement to be valid for the effective radius. We find, however, that the exponent 2 fits the results for the dynamics of the longest finger better than the exponent 1.64.

We have compared our results with the DLA simulations described above. The simulations were carried out on a hexagonal lattice with the outer boundary having a radius of 200 lattice units. The results shown in Fig. 6 are the average from 20 simulations. We find the good agreement between the simulations and the observed dynamics of the longest finger very satisfying.

The mean radius of the active zone as a function of time has also been measured. Here the active zone was approximated by the growth increment between two successive pictures. Similar approximations to the active zone have been used to analyze the results of computer simulations.[24]

The mean radius of the active zone is defined as

$$l = \frac{1}{n} \Sigma l_i \ , \tag{5}$$

where l_i is the distance from the center of injection to one black pixel on the growth zone and n is the total mass of the growth zone. The result of three experiments with air injected into glycerol with the same pressure difference $p_s - p_0 = 20.2$ mm Hg is shown in Fig. 7.

Since l describes the growth of the cluster, it must be related to the fractal dimension D of the frozen structure. If the mean radius from the same data is plotted as a function of the radius of gyration R_g of the viscous finger structure of the last picture, we obtain the result shown in Fig. 8. In the same figure we have also plotted the longest finger as a function of the gyration radius of the total cluster for the same experiments. Linear functions shown as a solid lines in Fig. 8 fit the data points well. Within the accuracy of our experiment the mean radius of the growth zone, the longest finger, and the radius of gyration of the total cluster have the same functional form:

$$l = c_1 R_g \sim r_m = c_2 R_g \sim N_0^{1/D} \ . \tag{6}$$

The values of the constants c_1 and c_2 from fitting to linear functions are $c_1 = 1.49 \pm 0.02$ and $c_2 = 1.98 \pm 0.03$. This result is consistent with the DLA simulation of Plischke and Rácz,[14] who found the same exponent $1/D$ for both l and R_g as a function of N_0.

The gyration radius of the growth zone l_g is defined as

$$l_g = \left[\frac{1}{n} \Sigma l_i^2 \right]^{1/2} \ . \tag{7}$$

The relationship between the width of the active zone (the screening width) and the radius of gyration has been a

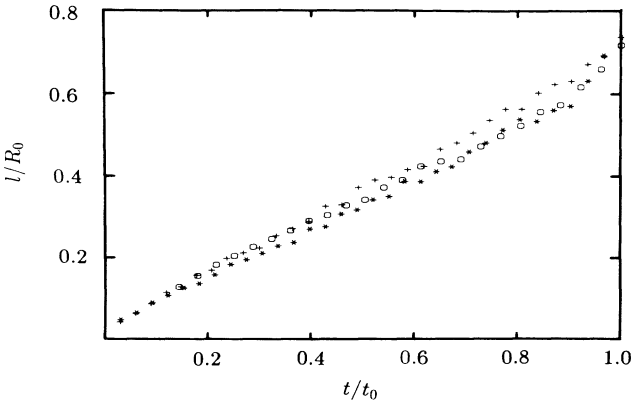

FIG. 7. Mean radius l/R_0 of the active zone as a function of time t/t_0 from three different experiments where air displaces glycerol. The pressure difference $(p_s - p_0)$ was 20.2 mm Hg in all three experiments.

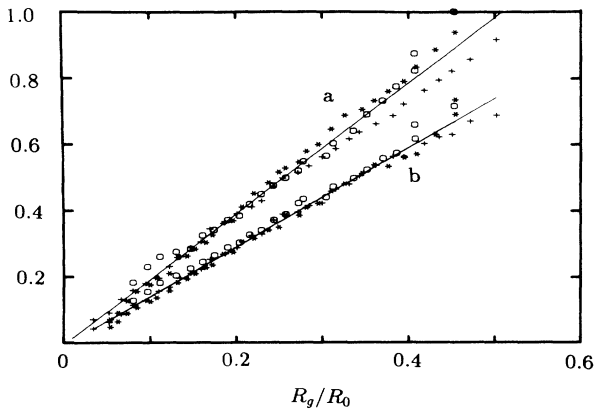

FIG. 8. (a) The longest finger r_m/R_0 as a function of the radius of gyration R_g/R_0 for the same experiments used to obtain Fig. 7. (b) The mean radius l/R_0 of the active zone as a function of the radius of gyration R_g/R_0 of whole cluster for the three experiments used to obtain Fig. 7. These results were obtained with air displacing glycerol. The pressure difference (p_s-p_0) was 20.2 mm Hg.

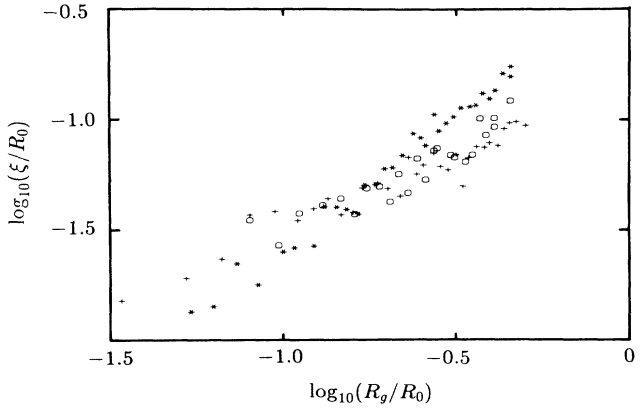

FIG. 10. Width of the active zone ξ/R_0 as a function of the gyration radius R_g/R_0 obtained from the three experiments used to obtain Fig. 7. The pressure difference was (p_s-p_0) of 20.2 mm Hg, with air displacing glycerol.

subject of considerable interest.[14,23–27] The width of the growth zone is defined as

$$\xi=(l^2-l_g^2)^{1/2} . \tag{8}$$

We have measured this quantity as a function of time and the result of one of these measurements is shown in Fig. 9.

When we plotted ξ as a function of the gyration radius R_g of the whole cluster, we found different slopes from different experiments. Comparing the results of different experiments, we found that clusters with the highest number of major branches had a lower slope than clusters with fewer major branches. This indicates that the screening width is sensitive to the number of major branches.

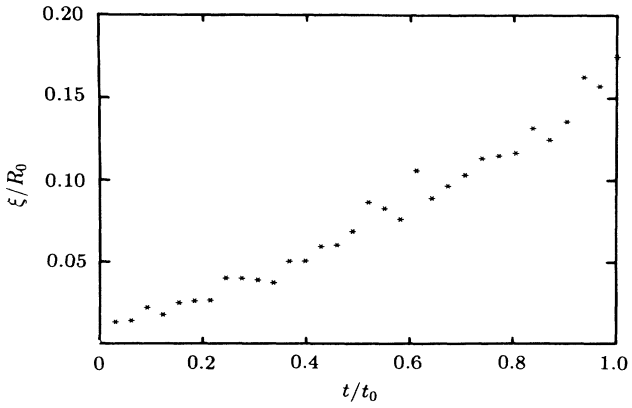

FIG. 9. Width of the active zone ξ/R_0 as a function of time t/t_0. The pressure difference was (p_s-p_0) of 20.2 mm Hg, with air displacing glycerol.

Plischke and Rácz[25] argue that since DLA clusters scale differently in the radial and tangential directions, the width of the active zone should scale differently from the radius of gyration of the total cluster. They suppose that the screening depth is proportional to the mean distance between the branches. From their simulation[14] of clusters containing 10 000 particles they found $\alpha=0.83$, where α is the exponent which relates the width of the active zone (ξ) to the radius of gyration (R_g) according to

$$\xi\sim R_g^{\alpha} . \tag{9}$$

Meakin and Sander[23] found that when the size of the cluster increased the exponent α increased. By using 1000 off-lattice clusters, each containing 50 000 particles, they found that the effective value of α increased with increasing cluster size. For clusters containing 50 000 particles they found that $\alpha=0.93$ and suggested that the limiting value for $(N_0\to\infty)$ should be 1.0. The asymptotic value for the exponent α is still un unresolved question. In Fig. 10 we have plotted ξ as a function of R_g for three different experiments in a double logarithmic plot. There is too much noise in our data to give an answer to this question. If we assume a power-law behavior $(\xi\sim R_g^{\alpha})$, the exponent α lies between 0.8 and 1.2 for our data.

V. DISCUSSION

The dynamic properties of viscous fingers with fractal dimension 1.64±0.04 in the DLA regime have been studied. The growing cluster is screened by the longest fingers. We have measured the longest finger as function of time and found that the data fit very well to DLA simulations. Our results have also been compared with the analytical expression for a growing bubble, Eq. (4).

Both the mean radius l of the growth zone and the length of the longest finger r_m are proportional to the gyration radius R_g of the total cluster. l, r_m, and R_g therefore follow the same scaling law $l\sim R_g\sim r_m\sim N_0^{1/D}$.

The result $l \sim N_0^{1/D}$ has also been found in DLA simulations by Plischke and Rácz.

Our statistical uncertainties were too large to resolve experimentally the question concerning the relationship between the width of the active zone (ξ) and the mean radius of the active zone or the radius of gyration. Additional experiments will be carried out in an attempt to reduce these uncertainties.

ACKNOWLEDGMENTS

We thank Amnon Aharony for stimulating and useful discussions. This research has been supported by VISTA, a research cooperation between the Norwegian Academy of Science and Letters (Vitenskapsakademiet) and Den Norske Stats Oljeselskap (STATOIL). One of us (K.J.M.) wishes to acknowledge the support of STATOIL.

[1]J. D. Chen and D. Wilkinson, Phys. Rev. Lett. **55**, 1892 (1985).
[2]K. J. Måløy, J. Feder, and T. Jøssang, Phys. Rev. Lett. **55**, 2688 (1985).
[3]B. B. Mandelbrot, *The Fractal Geometry of Nature* (Freeman, San Francisco, 1982).
[4]T. A. Witten and L. M. Sander, Phys. Rev. Lett. **47**, 1400 (1981).
[5]J. Nittmann, G. Daccord, and H. E. Stanley, Nature **314**, 141 (1985).
[6]L. Paterson, Phys. Rev. Lett. **52**, 1621 (1984).
[7]L. P. Kadanoff, J. Stat. Phys. **39**, 267 (1985).
[8]L. Niemeyer, L. Pietronero, and A. J. Wiesmann, Phys. Rev. Lett. **52**, 1033 (1984).
[9]M. Matsushita, M. Sano, Y. Hayakawa, H. Honjo, and Y. Sawada, Phys. Rev. Lett. **53**, 286 (1984).
[10]R. M. Brady and R. C. Ball, Nature **309**, 225 (1984).
[11]W. T. Elam, S. A. Wolf, J. Sprague, D. V. Gubser, D. Van Vechten, G. L. Barz, Jr., and P. Meakin, Phys. Rev. Lett. **54**, 701 (1985).
[12]H. Honjo, S. Ohta, and M. Matsushita, J. Phys. Soc. Jpn. **55**, 2487 (1986).
[13]G. Daccord, Phys. Rev. Lett. **58**, 479 (1987); G. Daccord and R. Lenormand, Nature **325**, 41 (1987).
[14]M. Plischke and Z. Rácz, Phys. Rev. Lett. **53**, 415 (1984).
[15]J. M. Deutch and P. Meakin, J. Chem. Phys. **78**, 2093 (1983).
[16]H. G. E. Hentschel, J. M. Deutch, and P. Meakin, J. Chem. Phys. **81**, 2496 (1984).
[17]P. Meakin and J. M. Deutch, J. Chem. Phys. **80**, 2115 (1984).
[18]R. F. Voss, Phys. Rev. B **30**, 334 (1984).
[19]P. Meakin, Phys. Rev. A **33**, 3371 (1986).
[20]P. Meakin, J. Phys. A **18**, L661 (1985).
[21]P. G. Saffman and G. Taylor, Proc. R. Soc. London, Ser. A **245**, 312 (1958).
[22]L. Paterson, J. Fluid Mech. **113**, 513 (1981).
[23]P. Meakin and L. M. Sander, Phys. Rev. Lett. **54**, 2053 (1985).
[24]P. Meakin, Phys. Rev. A **32**, 453 (1985).
[25]M. Plischke and Z. Rácz, Phys. Rev. Lett. **54**, 2054 (1985).
[26]G. Daccord, J. Nittmann, and H. E. Stanley, Phys. Rev. Lett. **56**, 336 (1986).
[27]M. Plischke and Z. Rácz, Phys. Rev. A **31**, 985 (1984).